





Targeted A and B site double doping in LaMnO₃ perovskites nanoparticles: Tailoring the magnetic behaviour for spintronic applications

G. Sheeba Sharon^a, M. Kumaresavanji^a , M. Baneto^{b,c}, K. Ravichandran^d, K. Sofiya^e , S. Ravi^a, A.T. Ravichandran^{a,*}

^a PG and Research Department of Physics, National College (Autonomous), Affiliated to Bharathidasan University, Tiruchirappalli, 620 001, Tamil Nadu, India

^b Department of Physics, University of Lomé, 01BP1515, Lomé, Togo

^c Regional Center of Excellence for Electricity Management (CERME), University of Lomé, 01BP1515, Lomé, Togo

^d PG and Research Department of Physics, AVVM Sri Pushpam College (Autonomous), (Affiliated to Bharathidasan University, Tiruchirappalli), Poondi, Thanjavur, 613 503, Tamil Nadu, India

^e Department of Chemical Engineering, School of Bio Engineering, College of Engineering and Technology, SRM Institute of Science and Technology, Kattankulathur, 603 203, Tamil Nadu, India

ARTICLE INFO

Keywords:

LaMnO₃
Perovskites
A- site B- site doping
Solution combustion synthesis
Magnetic properties
Spintronics

ABSTRACT

This study reports the synthesis and characterization of A-site and B-site doped perovskites nanoparticles La_{0.8}Sr_{0.1}Ca_{0.1}MnO₃ and LaMn_{0.8}Fe_{0.1}Co_{0.1}O₃ prepared using cost-effective solution combustion synthesis with oxalic acid as fuel. X-ray diffraction profile confirms tetragonal symmetry for both La_{0.8}Sr_{0.1}Ca_{0.1}MnO₃ and LaMn_{0.8}Fe_{0.1}Co_{0.1}O₃. The FESEM study showed particle agglomeration with average sizes of 75 and 67 nm, attributed to ionic radii differences. Elemental composition was verified through EDX analysis. Magnetic measurements conducted at 5 and 300 K demonstrate that La_{0.8}Sr_{0.1}Ca_{0.1}MnO₃ displayed soft magnetic properties with high saturation magnetization (79.81 emu/g) and low coercivity (0.016 T), whereas LaMn_{0.8}Fe_{0.1}Co_{0.1}O₃ showed hard magnetic characteristics with increased coercivity (0.38 T) and lower saturation magnetization (51.25 emu/g). Temperature-dependent magnetization studies showed ferromagnetic to paramagnetic transitions for both materials, suggesting that targeted doping at A- and B-sites enhances magnetic performance. The findings suggest the materials' potential applications in spintronic devices such as magnetic storage and sensors.

1. Introduction

Spintronics offers promising advancements for energy-efficient devices by utilizing both electron charge and spin, essential in applications like magnetic tunnel junctions (MTJ), spin valves, giant magnetoresistive sensors (GMR), spin-based transistors, and quantum dots [1–3]. Perovskite materials specifically LaMnO₃, stand out for their versatility, with doping at either the A-site, B-site, or both, enhancing various properties, such as magnetoresistance and magnetic transitions, making them suitable for various applications including catalysis, thermoelectrics, supercapacitors, electrochemical sensors, magnetic devices and biomedical applications [4–8]. Among the various methods available for the perovskite synthesis, solution combustion synthesis is widely recognized for its simplicity and cost-effectiveness [9].

In this study, LaMnO₃ nanoparticles were synthesized via solution combustion synthesis with targeted A-site and B-site double doping to

alter the structural and magnetic characteristics. For A-site, Sr and Ca and for B-site, Fe and Co were used as co-dopants. The structural changes and the consequent alterations in the magnetic behaviour of the resultant double-doped perovskites viz. La_{0.8}Sr_{0.1}Ca_{0.1}MnO₃ and LaMn_{0.8}Fe_{0.1}Co_{0.1}O₃ were studied and reported.

2. Experimental details

The chemical reagents lanthanum nitrate hexahydrate (La(NO₃)₃·6H₂O), calcium nitrate tetrahydrate (Ca(NO₃)₂·4H₂O), strontium nitrate anhydrous (Sr(NO₃)₂), manganese(II) nitrate tetrahydrate (Mn(NO₃)₂·4H₂O), ferric nitrate (Fe(NO₃)₃·9H₂O), cobalt nitrate hexahydrate (Co(NO₃)₂·6H₂O) are the oxidizers and oxalic acid (C₂H₂O₄·2H₂O) is the fuel/reducing agent. They were used without further purification for the preparation of combusted La_{0.8}Sr_{0.1}Ca_{0.1}MnO₃ and LaMn_{0.8}Fe_{0.1}Co_{0.1}O₃ perovskite nanoparticles. The

* Corresponding author.

E-mail address: atrncet@gmail.com (A.T. Ravichandran).

<https://doi.org/10.1016/j.matlet.2025.138040>

Received 6 November 2024; Received in revised form 23 December 2024; Accepted 10 January 2025

Available online 11 January 2025

0167-577X/© 2025 Elsevier B.V. All rights are reserved, including those for text and data mining, AI training, and similar technologies.

oxidizer/fuel ratio was kept as 9:8 for former and 10:8 for the latter, according to the concept of propellant chemistry.

The LaMnO_3 perovskite nanoparticles were prepared using a simple solution combustion synthesis. To synthesize $\text{La}_{0.8}\text{Sr}_{0.1}\text{Ca}_{0.1}\text{MnO}_3$ nanoparticles, stoichiometric amounts of lanthanum, calcium, strontium and manganese nitrates along with oxalic acid were dissolved in deionized water. The solution was stirred and heated in a muffle furnace at 300 °C for combustion reaction, which produced a fluffy powder. Then the powder was calcined at 800 °C and ground. The same procedure was used to synthesize $\text{LaMn}_{0.8}\text{Fe}_{0.1}\text{Co}_{0.1}\text{O}_3$ nanoparticles.

3. Characterization

Structural analysis was carried out using powder X-ray diffraction (XRD) with $\text{CuK}\alpha$ radiation on an X'Pert Pro PANalytical Powder X-ray Diffractometer and the Rietveld refinement was done by using TOPAS software. The morphology of the nanoparticles was examined using a Carl Zeiss Sigma 300 Field Emission Scanning Electron Microscope (FESEM) coupled with an Energy Dispersive X-ray (EDX) spectrometer. ImageJ software was used to determine the average particle size of the samples. The X-ray Photoelectron Spectroscopy (XPS) analysis was performed to study the chemical state of the atoms present in the systems using an ULVAC PHI, model VersaProbe III in XPS mode. The temperature dependence of magnetization (M–T) was recorded in the temperature range of 5 to 350 K under an applied magnetic field of 100 Oe. Field-dependent magnetization (M–H) was measured at 5 and 300 K with a maximum applied field of 6 T. All magnetic measurements were carried out using a Quantum Design DynaCool PPMS.

4. Results and discussion

4.1. XRD, FESEM and EDX studies

The Fig. 1. (a and b) show the rietveld-refined patterns along with their three-dimensional crystal structures of $\text{La}_{0.8}\text{Sr}_{0.1}\text{Ca}_{0.1}\text{MnO}_3$ and $\text{LaMn}_{0.8}\text{Fe}_{0.1}\text{Co}_{0.1}\text{O}_3$ nanoparticles, respectively which confirm the formation of tetragonal crystal system with I4/mcm space group. The refined patterns display a close overlap of observed (Yobs) and calculated (Ycalc) peaks, with their difference (Yobs – Ycalc) shown in blue, indicating a good structural fit, confirming the perovskite structure of these compounds. The 3D crystal structure obtained through refinement clearly shows the substitutional incorporation of the dopant ions Sr and Ca into the regular sites of La as seen in Fig. 1. (a). Similarly, the substitutional incorporation of Fe and Co into the regular sites of Mn in the LaMnO_3 lattice is illustrated in Fig. 1. (b). The shorter Mn-O bond length and larger Mn-O-Mn bond angle in $\text{La}_{0.8}\text{Sr}_{0.1}\text{Ca}_{0.1}\text{MnO}_3$ favour strong ferromagnetic properties. In contrast, longer Mn-O bond length and smaller Mn-O-Mn bond angle in $\text{LaMn}_{0.8}\text{Fe}_{0.1}\text{Co}_{0.1}\text{O}_3$ result in weaker ferromagnetic properties. The obtained bond angle, bond length, R-factors, GOF values, lattice parameters, atomic positions, occupancies and crystallite size are presented in the tables ST1 and ST2.

The FESEM images (Fig. 2. a and b) highlight the particle size

differences between $\text{La}_{0.8}\text{Sr}_{0.1}\text{Ca}_{0.1}\text{MnO}_3$ and $\text{LaMn}_{0.8}\text{Fe}_{0.1}\text{Co}_{0.1}\text{O}_3$ nanoparticles, with average sizes of 75 and 67 nm. Both samples show agglomeration due to the gases evolved during combustion and the larger ionic radii of Sr^{2+} and Ca^{2+} . However, $\text{LaMn}_{0.8}\text{Fe}_{0.1}\text{Co}_{0.1}\text{O}_3$ displays more uniform particles with clear boundaries due to the smaller ionic radii of Fe^{3+} and Co^{3+} . The EDX spectra (Fig. 2. c and d) confirm the presence of expected elements in the samples.

4.2. PPMS analysis

The field dependence of magnetization (M–H) at a temperature of 5 and 300 K for both $\text{La}_{0.8}\text{Sr}_{0.1}\text{Ca}_{0.1}\text{MnO}_3$ and $\text{LaMn}_{0.8}\text{Fe}_{0.1}\text{Co}_{0.1}\text{O}_3$ nanoparticles is illustrated in Fig. 3a, highlighting distinct magnetic behaviours. At 5 K, $\text{La}_{0.8}\text{Sr}_{0.1}\text{Ca}_{0.1}\text{MnO}_3$ shows a sharp rise in magnetization at low magnetic fields (up to 0.5 T), reaching saturation magnetization (M_s) at 79.81 emu/g. The narrow hysteresis loop, with a very small coercivity (H_c) of 0.016 T indicates soft ferromagnetic material. The remanent magnetization (M_r) at 12.71 emu/g shows that the material retains a small fraction of its magnetization even after the external field is removed. Conversely, $\text{LaMn}_{0.8}\text{Fe}_{0.1}\text{Co}_{0.1}\text{O}_3$ shows a broader hysteresis loop, indicating higher coercivity (0.38 T) and a lower saturation magnetization (51.25 emu/g) with higher remanent magnetization (28.33 emu/g), indicating hard ferromagnetic behaviour, with significant retention of magnetization. At 300 K, $\text{La}_{0.8}\text{Sr}_{0.1}\text{Ca}_{0.1}\text{MnO}_3$ shows a reduced M_s (39.79 emu/g), M_r (0.34 emu/g) and H_c (0.005 T) suggesting weaker ferromagnetic behaviour. The $\text{LaMn}_{0.8}\text{Fe}_{0.1}\text{Co}_{0.1}\text{O}_3$ nanoparticles shows a linear response revealing the paramagnetic behaviour. These variations in the magnetic behaviour are caused by the substitutional incorporation of the two different pairs of co-dopants (Sr & Ca and Fe & Co) at the sites of the host elements La and Mn as confirmed by the Rietveld refinement results.

The temperature dependence of magnetization (M–T) under zero-field cooled (ZFC) and field cooled (FC) conditions at a field of 100 Oe for $\text{La}_{0.8}\text{Sr}_{0.1}\text{Ca}_{0.1}\text{MnO}_3$ and $\text{LaMn}_{0.8}\text{Fe}_{0.1}\text{Co}_{0.1}\text{O}_3$ nanoparticles is presented in Fig. 3b. For $\text{La}_{0.8}\text{Sr}_{0.1}\text{Ca}_{0.1}\text{MnO}_3$, the ZFC magnetization increases with temperature, reaching a peak at 261 K. The FC curve shows higher magnetization at low temperatures, gradually decreasing with temperature showing that the material exhibits ferromagnetic to paramagnetic transition. For $\text{LaMn}_{0.8}\text{Fe}_{0.1}\text{Co}_{0.1}\text{O}_3$, the FC magnetization begins at 8.32 emu/g and remains relatively constant till 48 K, then decreasing sharply which indicates that the material exhibits ferromagnetic behaviour. As the temperature increases, the flattening of the curve suggests that the material becomes paramagnetic. The ZFC curve rises until 95 K and sharply decreases and flattens at 129 K, indicating a similar transition. The Curie temperatures (T_c) were found to be 300.35 K for $\text{La}_{0.8}\text{Sr}_{0.1}\text{Ca}_{0.1}\text{MnO}_3$ and 107.09 K for $\text{LaMn}_{0.8}\text{Fe}_{0.1}\text{Co}_{0.1}\text{O}_3$ nanoparticles.

5. Proposed mechanism

The proposed mechanism is illustrated in Fig. 4. In $\text{La}_{0.8}\text{Sr}_{0.1}\text{Ca}_{0.1}\text{MnO}_3$, the substitution of Sr^{2+} and Ca^{2+} into the La^{3+} regular site

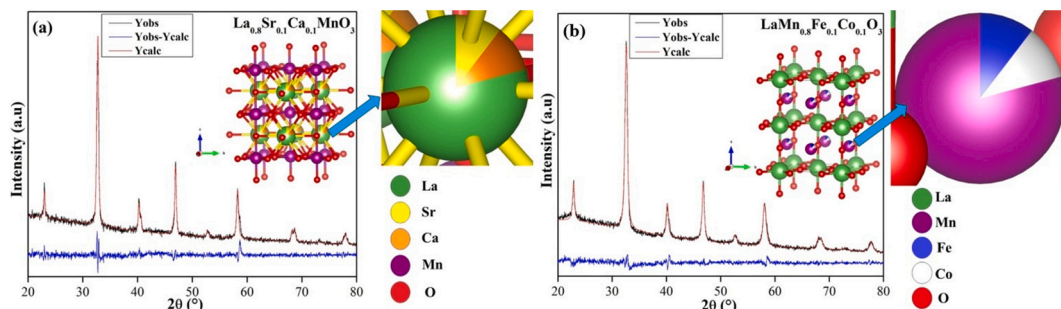


Fig. 1. (a and b) Refined XRD patterns with 3D crystal structures of the samples.

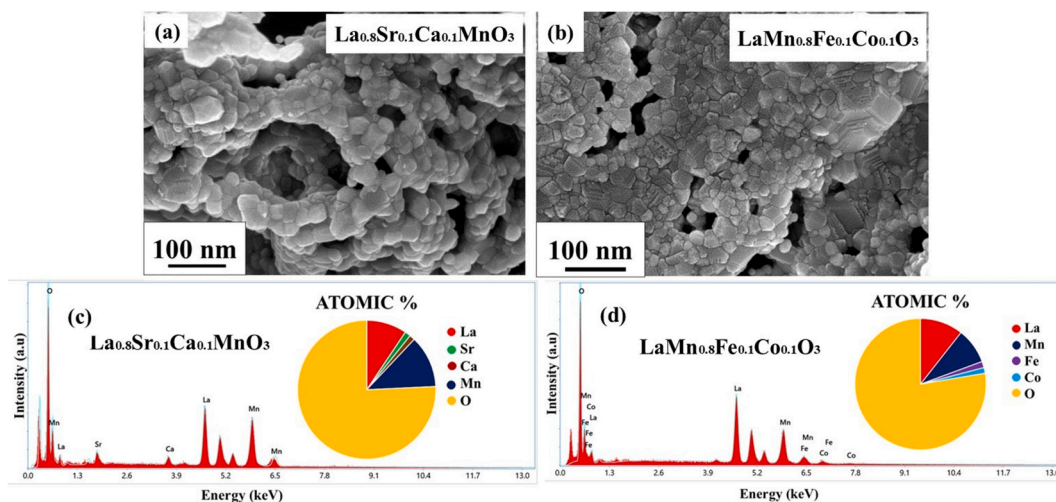


Fig. 2. (a and b) FESEM images and (c and d) EDX spectra (inset- atomic percentages of elements) of the samples.

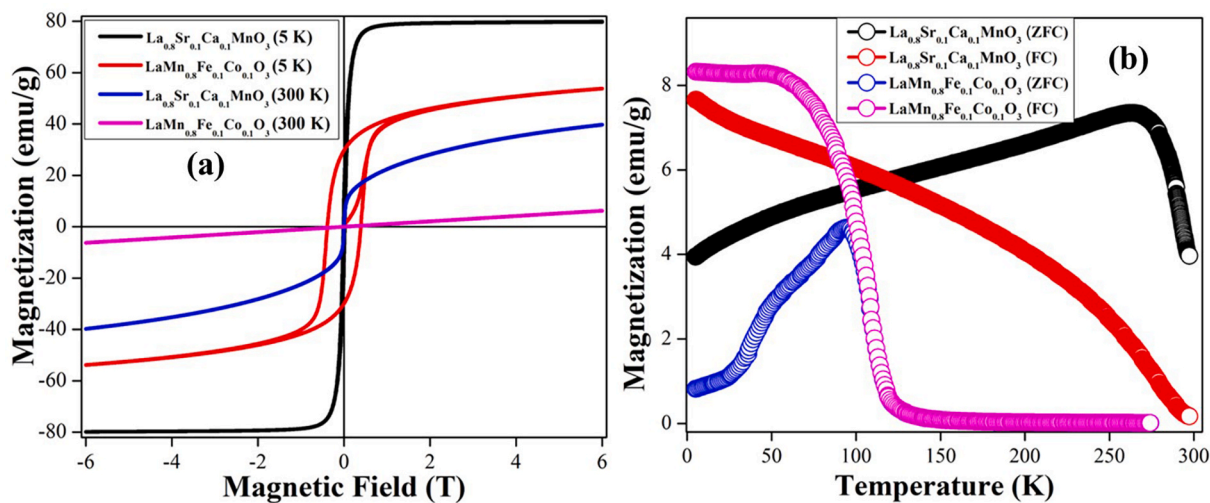


Fig. 3. Magnetization vs Magnetic field (M vs H) and Magnetization vs Temperature (M vs T) curves of $\text{La}_{0.8}\text{Sr}_{0.1}\text{Ca}_{0.1}\text{MnO}_3$ and $\text{LaMn}_{0.8}\text{Fe}_{0.1}\text{Co}_{0.1}\text{O}_3$ nanoparticles.

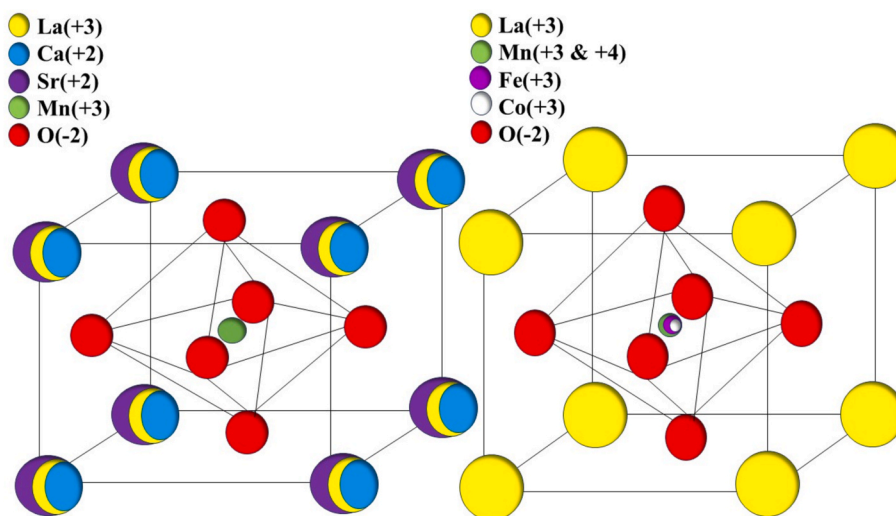


Fig. 4. Proposed mechanism for the magnetic behaviour of $\text{La}_{0.8}\text{Sr}_{0.1}\text{Ca}_{0.1}\text{MnO}_3$ and $\text{LaMn}_{0.8}\text{Fe}_{0.1}\text{Co}_{0.1}\text{O}_3$ nanoparticles.

ensures charge neutrality and influences the material's magnetic properties, while predominantly maintaining Mn^{3+} as evidenced by the XPS spectra given in the [supplementary file](#). In $LaMn_{0.8}Fe_{0.1}Co_{0.1}O_3$, Fe^{3+} and Co^{3+} substitute Mn at the B-site creates a mixed valence state, which influences the electron configuration and alter its magnetic order. These dopants in both compounds contribute to variations in their magnetic behaviour.

6. Conclusion

The A-site ($La_{0.8}Sr_{0.1}Ca_{0.1}MnO_3$) and B-site ($LaMn_{0.8}Fe_{0.1}Co_{0.1}O_3$) double-doped $LaMnO_3$ nanoparticles synthesized using solution combustion synthesis with oxalic acid as fuel exhibited different magnetic properties. The XRD analysis confirmed that $La_{0.8}Sr_{0.1}Ca_{0.1}MnO_3$ and $LaMn_{0.8}Fe_{0.1}Co_{0.1}O_3$ have a tetragonal structure with I4/mcm space group. The FESEM images indicated particle agglomeration with average particle size of 75 and 67 nm and the EDX confirmed the presence of expected constituent elements in the respective systems. Magnetic measurements showed notable differences in magnetic behaviour between the samples. The $La_{0.8}Sr_{0.1}Ca_{0.1}MnO_3$ exhibited strong ferromagnetic behavior with soft magnetic properties showing high saturation magnetization of 79.81 emu/g and low coercivity of 0.016 T, whereas $LaMn_{0.8}Fe_{0.1}Co_{0.1}O_3$ displayed hard magnetic behaviour with higher coercivity (0.38 T) and lower saturation magnetization (51.25 emu/g) at 5 K. Temperature-dependent magnetization (M–T) studies revealed the ferromagnetic to paramagnetic transitions in both the materials, with distinct transition temperatures. The results demonstrate that tailored A- site and B-site doping in $LaMnO_3$ can significantly alters the magnetic properties, indicating promising potential for applications in spintronic devices like magnetic storage and sensors.

CRediT authorship contribution statement

G. Sheeba Sharon: Writing – original draft, Funding acquisition, Data curation, Conceptualization. **M. Kumaresavanji:** Writing – review & editing. **M. Baneto:** Writing – review & editing. **K. Ravichandran:** Writing – review & editing, Validation. **K. Sofiya:** Writing – review & editing, Validation. **S. Ravi:** Supervision. **A.T. Ravichandran:** Writing – review & editing, Validation.

Declaration of competing interest

The authors declare that they have no known competing financial interests or personal relationships that could have appeared to influence the work reported in this paper.

Appendix A. Supplementary data

Supplementary data to this article can be found online at <https://doi.org/10.1016/j.matlet.2025.138040>.

Data availability

Data will be made available on request.

References

- [1] A. Hirohata, K. Yamada, Y. Nakatani, I. Prejbeanu, B. Diény, P. Pirro, B. Hillebrands, Review on spintronics: Principles and device applications, *J. Magn. Magn. Mater.* 509 (2020) 166711, <https://doi.org/10.1016/j.jmmm.2020.166711>.
- [2] A. Hirohata, K. Takanashi, Future perspectives for spintronic devices, *J. Phys. D Appl. Phys.* 47 (19) (2014) 193001, <https://doi.org/10.1088/0022-3727/47/19/193001>.
- [3] A. Murtaza, W. Zuo, X. Song, A. Ghani, A. Saeed, M. Yaseen, F. Tian, S. Yang, Robust ferromagnetism in rare-earth and transition metal co-doped ZnO nanoparticles for spintronics applications, *Mater. Lett.* 310 (2021) 131479, <https://doi.org/10.1016/j.matlet.2021.131479>.
- [4] R. Spinicci, M. Faticanti, P. Marini, S. De Rossi, P. Porta, Catalytic activity of $LaMnO_3$ and $LaCoO_3$ perovskites towards VOCs combustion, *Journal of Molecular Catalysis a Chemical* 197 (1–2) (2003) 147–155, [https://doi.org/10.1016/s1381-1169\(02\)00621-0](https://doi.org/10.1016/s1381-1169(02)00621-0).
- [5] M. Abdolrahmani, M. Parvari, M. Habibpoor, Effect of Copper Substitution and Preparation Methods on the $LaMnO_{3\pm\delta}$ Structure and Catalysis of Methane Combustion and CO Oxidation, *Chin. J. Catal. (chinese Version)* 31 (4) (2010) 394–403, [https://doi.org/10.1016/s1872-2067\(09\)60059-0](https://doi.org/10.1016/s1872-2067(09)60059-0).
- [6] L. Rivera-Rios, I.O. Perez-Lopez, J.T. Elizalde-Galindo, J.R. Farias-Mancilla, P. G. Mani-Gonzalez, Doping lanthanum manganites particles with strontium-calcium for application in hyperthermia, *J. Appl. Res. Technol.* 20 (4) (2022) 481–486, <https://doi.org/10.22201/icat.24486736e.2022.20.3.1405>.
- [7] Y. Liu, H. Wong, S. Huang, S. Hu, S. Ng, K. Lam, C. Mak, C. Leung, Structural, magnetic and transport properties of fully epitaxial $LaMnO_3/LaAlO_3$ multilayers, *Mater. Lett.* 205 (2017) 230–232, <https://doi.org/10.1016/j.matlet.2017.06.097>.
- [8] H. Wang, C. Yang, K. Su, S. Huang, D. Huo, Structure and magnetic properties of epitaxial Pt/ $LaMnO_3$ bilayer, *Mater. Lett.* 236 (2018) 152–154, <https://doi.org/10.1016/j.matlet.2018.10.092>.
- [9] K.C. Patil, S. Aruna, T. Mimani, Combustion synthesis: an update, *Curr. Opin. Solid State Mater. Sci.* 6 (6) (2002) 507–512, [https://doi.org/10.1016/s1359-0286\(02\)00123-7](https://doi.org/10.1016/s1359-0286(02)00123-7).